TILT ROTOR ANALYSIS AND DESIGN USING FINITE-ELEMENT MULTIBODY PROCEDURES

Carlo L. Bottasso, Lorenzo Trainelli
Dipartimento di Ingegneria Aerospaziale, Politecnico di Milano, Milano, Italy

Pierre Abdel-Nour, Gianluca Labò
Agusta S.p.A., Cascina Costa di Samarate, Varese, Italy

Abstract

The present work focuses on the application of the finite-element multibody technique to the dynamic analysis of tilt rotors. A detailed multibody model is first described and validated against well established solution procedures. The non-linear model developed herein includes a full description of the control linkages and three possible realizations of the gimbal mount. The effects of the three gimbal joint design solutions on the stability of the system are analyzed with the help of numerical simulations.

Introduction

New rotorcraft configurations can pose stringent modeling requirements, not easily met with standard simulation procedures. For example, tilt rotors present a number of unique features that set them apart from classical helicopter rotors: highly twisted blades, large pitch excursions across the flight envelope, gimbal mounts that allow the flapping of the rotor while at the same time try to provide a constant transmission of the angular velocity. Lack of detail in some of these critical components, or questionable "equivalent" or linearized models, can seriously undermine the reliability of the analysis and its final effectiveness in the design process. It is clear that the overall accuracy delivered by an aeroelastic model will depend on the accuracy of its components, such as the structural dynamics model, the aerodynamic model, the possible controls model, the coupling strategy, etc. On the structural dynamics side of the problem, it is now possible to use more kinematically and dynamically consistent non-linear models than it was usually done in the past.

In fact, multibody formulations can deal with complex flexible mechanisms of arbitrary topologies. Using this approach, a given mechanism is modeled through an idealization process that identifies the mechanism components from within a large library of elements implemented in a software code. Each element provides a basic functional building block, for example a rigid or flexible member, a hinge, a motor, etc. After assembling the various elements, one can construct a virtual prototype of the mechanism with the required level of accuracy. Therefore, using this technology one can model a complex system such as a tilt rotor with a higher level of detail than it is presently possible using conventional industrial tools.

In ref. [1], a multibody simulation procedure was proposed that is applicable to rotorcraft systems and that provides a comprehensive, modular and expandable simulation software. The same code was demonstrated on the aeroelastic analysis of engage and disengage operations in high wind conditions for a detailed model of an articulated rotor in ref. [4] and ref. [2]. The multibody dynamics analysis is cast within the framework of non-linear finite element methods, and the element library includes rigid and deformable bodies as well as joint elements. Deformable bodies are modeled with the finite element method, in contrast with the classical approach that predominantly relies on rigid bodies or introduces flexibility by means of a modal representation.

In this work we use the multibody finite element approach for modeling a tilt rotor, considering the details of the control linkages and of the gimbal mount. The system here considered is the Agusta Erica concept, an on-going project for an innovative tilt rotor in the 10 ton, 20 seat class. At first, a validation is carefully carried out by comparison with established industrial codes, including NASTRAN [6] and CAMRAD/JA [5]. The validation effort includes modal analyses at different rotor speeds in aircraft and helicopter mode, and comparisons of the rotor aerodynamic loads in different flight conditions.

Next, we use the high fidelity kinematic and dynamic modeling capability of the multibody approach for studying the influence of the possible effects of the geometric non-linearities related to the hub design on the whirl-flutter stability. We discuss three possible models of the gimbal mount. First, we consider a simple mount represented by a standard universal (Hooke) joint, which is not a constant speed joint. Next, we study a more interesting joint that guarantees an exact constant speed transmission only in certain operating conditions. This joint is again modeled as a multibody system, using a variety of joints and rigid bodies. Finally, we investigate an "ideal" joint that realizes an exact constant speed transmission in all flight conditions. The effects of these various realizations of the gimbal mounts on flutter limits are discussed in detail.

We conclude the paper with a plan of future activities, that include in particular the analysis of the drive train torsional loads and of the overall vibratory level.

Overview of the Finite Element Multibody Code

The basic features of the finite element multibody code used in this work are briefly reviewed in the following.

The element library includes the basic structural elements such as rigid bodies, composite capable beams and shells, and joint models. All elements are referred to a single inertial frame, and hence, arbitrarily large displacements and finite rotations are treated exactly. In this formulation, no modal reduction is performed, and the full finite element equations are used at all times. A finite element based cross-sectional analysis procedure is fully integrated with the multibody dynamics code and ensures the ability to model components made of laminated composite materials.

Joints are modeled through the use of appropriate holonomic or non-holonomic constraints enforced by means of Lagrange multipliers. All joints are formulated with the explicit definition of the relative joint motion as additional unknown variables. This allows the introduction of generic spring and/or damper elements in the joints, as usually required for the modeling of realistic configurations. Furthermore, the time histories of joint relative motions can be driven according to suitably specified time functions. All joints can be equipped with backlash, freeplay and friction models.

The code implements implicit integration procedures that are non-linearly unconditionally stable. The proof of non-linear unconditional stability stems from two physical characteristics of multibody systems that are reflected in the numerical scheme at the discrete level: the preservation of the total mechanical energy and the vanishing of the work performed by constraint forces. Numerical dissipation is obtained by letting the solution drift from the constant energy manifold in a controlled manner in such a way that at each time step, energy can be dissipated but not created. More details on these non-linearly stable schemes can be found in the bibliography of ref. [1].

Once a multibody representation of a system has been defined, several types of analyses can be performed on the virtual prototype. A *static* analysis solves the static equations of the problem, obtained by setting all time derivatives to zero. The deformed configuration of the system under the applied static loads is then computed. The static loads can be of various types, such as prescribed static loads, steady aerodynamic loads, or the inertial loads associated with prescribed rigid body motions.

Once the static solution has been found, the dynamic behavior of small amplitude perturbations about this equilibrium configuration can be studied. This is done by first linearizing the dynamic equations of motion, then extracting the eigenvalues and eigenvectors of the resulting linear system. Finally, static analysis is also useful for providing the initial conditions to a subsequent dynamic analysis.

A *dynamic* analysis solves the non-linear equations of motion for the complete finite element multibody system. The initial conditions are taken to be at rest, or those corresponding to a previously determined static or dynamic equilibrium configuration. Automated time step size adaptivity is available to increase the efficiency and accuracy of the simulation.

An important aspect of the aeroelastic response of rotorcraft vehicles is the potential presence of instabilities which can occur both on the ground and in flight. The multibody code implements the implicit Floquet analysis method [3], which evaluates the dominant eigenvalues of the transition matrix using the Arnoldi algorithm, without the explicit computation of the same matrix, which is potentially very expensive for a direct finite element approach. This method is ideally suited for systems involving a large number of degrees of freedom.

Finally, various visualization and post-processing procedures, including animations and time history plots, are used to help the analyst during the model preparation phase and for the interpretation of the computed results.

Tilt Rotor Multibody Model

A topological view of the multibody model of the aircraft is symbolically given in fig. 1. The various mechanical components of the system are associated with the elements found in the library of the code. The model consist of the wing, engine and nacelle and of a detailed representation of the rotor. The rotor itself includes shaft, swashplate, pitch-links, constant speed joint, flex-beam, cuff and blade.

The swashplate is represented by two rigid bodies, rotating and non-rotating, connected by a revolute joint. The non-rotating lower swashplate is connected to the nacelle by means of a universal joint followed by a prismatic joint. The collective input signal is provided by prescribing the relative displacement of the prismatic joint, whereas the cyclic input signals are provided by prescribing the two relative rotations of the universal joint. The rotating upper swashplate is connected to the pitch-links by means of universal joints. In turn, the pitch-links are attached to the pitch-horn through

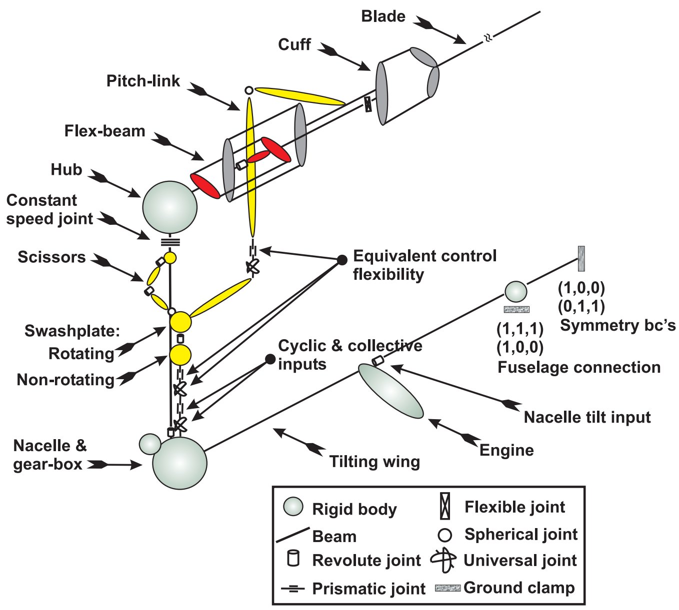

Figure 1: Topological representation of the tilt rotor multibody model. One single blade is depicted for clarity.

spherical joints and transfer the input control signals from the upper swashplate to the blades. The rotation of the upper swashplate is enforced by scissors that connect to the rotating shaft.

For this project, it was deemed necessary to model the flexibility of the control linkages in order to include this effect in the global aeroelastic model. At first, the flexibility measured at the head of the pitch-links was computed through a detailed finite element model of the whole control system. As commonly found in this case, the computed equivalent stiffness at this location depends on the type of load condition considered, namely cyclic, collective or reactionless. This effect was reproduced by introducing a special arrangement of additional joints with suitable stiffness characteristics. In particular, a prismatic joint is introduced in the pitch-links, whose stiffness represents the reactionless stiffness of the whole system. An additional prismatic joint followed by a universal joint is introduced immediately below the swashplate. The spring in this prismatic joint is computed so that its stiffness, in series with the springs of the pitch-links, yields a total stiffness of the system that is equal to the computed collective stiffness. Finally, the springs in the universal joints are computed in order to yield, again in series with the springs associated with the pitch-links, the cyclic stiffness of the system. This way, the load dependent stiffness characteristics of the control linkages can be modeled using just a few additional degrees of freedom. Furthermore, during the preliminary design phase the exact structural stiffness characteristics of each part of the control system are usually not known. This approach allows then to account for the control system compliance using just a few macro-parameters, as commonly done in this phase of the design.

Continuing in the description of the main components of the virtual model, we note that the shaft is attached to the hub, modeled as a massive rigid body, that in turn connects to a flex-beam, followed by the cuff and finally by the blade itself. Cuff and flex-beam are connected at two points through elastomeric joints and can rotate one with respect to the other to allow the blade pitch setting.

The wing model includes an inboard section which connects to the fuselage, and an outboard section that can be tilted by prescribing the relative rotation in a revolute joint that connects the two parts. Rigid bodies of appropriate inertial characteristics model the engine, nacelle and gear-box.

The aerodynamic model is based on lifting lines associated with each blade and parts of the cuff. The lifting lines are based on classical two-dimensional strip theory and use local profile aerodynamic characteristics, accounting for the aerodynamic center offset, twist, sweep, and unsteady corrections. The two-dimensional aerodynamic model is corrected through the use of the dynamic inflow model developed by Peters [7]. However, given the fact that we are here mainly interested in the whirl-flutter speed boundaries in airplane mode, the effects of an inflow model on the computed results is negligible.

The final multibody finite element model includes about 7,000 degrees of freedom, a clearly prohibitive size for classical Floquet analysis.

Constant-Speed Joint Models

The constant speed joint that connects shaft and hub was realized in three different versions. The first solution simply adopts a universal joint, which will provide a constant speed transmission only for null rotor flapping. The other two joints studied here represent an approximate and an ideal constant-speed joint which are described in detail in the next two sections.

The "Artichoke" Constant-Speed Joint Model

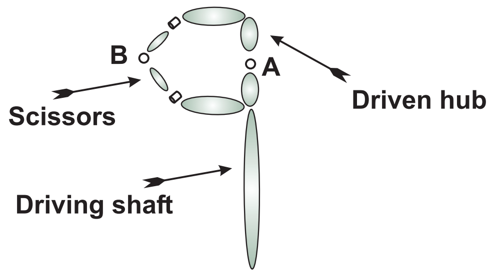

Figure 2: Topological model of the approximate constant speed joint.

The approximate constant speed joint is symbolically depicted in fig. 2. The driving shaft and hub are connected by a spherical joint (A) that allows the hub complete rotational freedom. Transmission of motion between shaft and hub is provided by a number of scissors. Each scissor is symmetric about the AB plane, which is normal to the shaft for null flapping. A spherical joint is used at B, while connections to shaft and hub are realized with revolute joints. The rotor blades are connected to the driven hub at the AB plane. Clearly, from a kinematical point of view one single scissor would be enough, and redundancy is here introduced only to distribute the resulting loads among a larger number of structural elements. Since there exists an alternative version of this joint using composite-made torque transfer petals that somehow resemble an artichoke, this joint will be called the "artichoke" in the following, for the sake of brevity.

This implementation of the constant speed link between shaft and hub is modeled using rigid bodies, revolute and spherical joints. Therefore it was easily introduced in the global model described in the previous section, and used for the aeroelastic simulations.

A second multibody model of the joint is depicted in fig. 3. This model is totally kinematically equivalent to the previous one; however, this second implementation allows to test the joint behavior independently of the rest of the rotor. This was done in order to try to give a preliminary characterization of the joint itself by means of numerical experiments. It is easily shown analytically that this joint will provide an exact constant speed transmission at the hub for arbitrary constant tilting of the hub normal with respect to a fixed reference frame, i.e. for constant tip plath plane; this is the same result that could be obtained by using two universal joints in series. However, the analytical characterization of the joint becomes quite complex for general motions of the hub normal, and a few numerical experiments can be helpful in clarifying its basic properties.

The spherical joint that allows the tilting of the hub in the first implementation is here replaced by a universal and a revolute joint in series, which are then connected to the ground. Testing of the model can then be conducted by explicitly tilting the hub through the prescribed rotations in the universal joint while spinning the shaft at some constant speed, and measuring the resulting angular speeds at the hub.

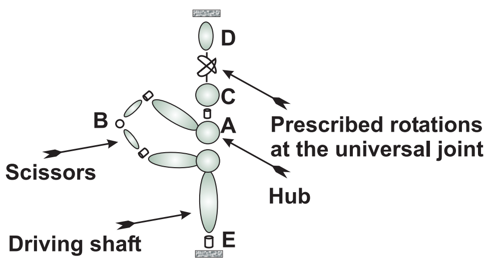

Figure 3: Topological model of the approximate constant speed joint used for its characterization.

We have conducted two tests with two different ways of tilting the hub: in the first test, the normal to the hub oscillates in a plane that contains the shaft axis, while in the second test the normal to the hub describes a cone. The shaft is driven by imposing a time history to the relative rotation at the revolute joint in E. Tilting of the hub is obtained by prescribing the time histories of the relative rotations in the universal joint. Note that the points labeled A, C and D in the figure are in reality coincident in the actual model. Rotations are measured and plotted at the driving revolute joint and at the revolute joint between points A and C. Angular velocities are measured in body attached axes and plotted for the driving shaft and the hub.

Example 1: Oscillations in a Plane

For this first case, one angle in the universal joint is described by a cosine function while the other is held fixed and null. The oscillation amplitude is 20 deg. with null mean value, while its speed is four times the angular speed of the driving shaft.

Fig. 4 gives the time history of the shaft rotations, of the universal joint rotations, and of the relative rotation in the revolute joint at point A. Fig. 5 gives the time history of the body attached components of angular velocity along the shaft axis and the hub normal. It is seen that the joint provides an exact constant speed transmission in this case.

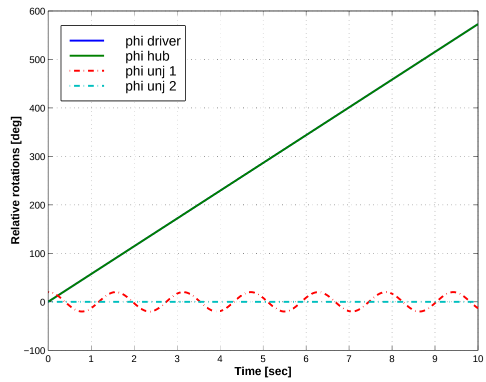

Figure 4: Oscillations in a plane: shaft rotations (solid lines), universal joint rotations (dash-dotted lines).

Example 2: Cone Motions

In this second case, a fully three-dimensional motion of the hub is considered. In particular, the normal to the hub plane exactly describes a cone of semi-aperture $\theta = 20$ deg. In order to achieve this result, one angle (ϕ_1) in the universal joint is described by a sine function while the other is computed as $\phi_2 = \mathrm{acos}(\cos(\theta)\cos(\phi_1))$. Since the number of blades for the Erica design is four, we use here a precession speed which is four times the angular speed of the driving shaft.

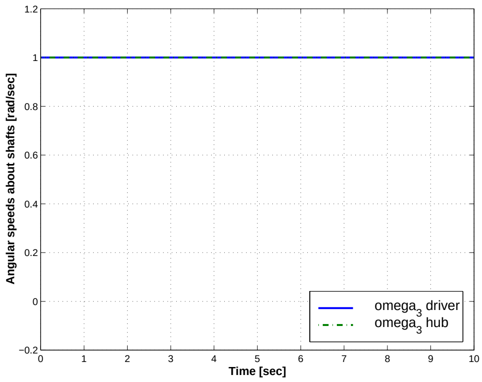

Figure 5: Oscillations in a plane: driving shaft angular speed ω_3^d (solid line), slave shaft angular speed ω_3^s (dash-dotted line).

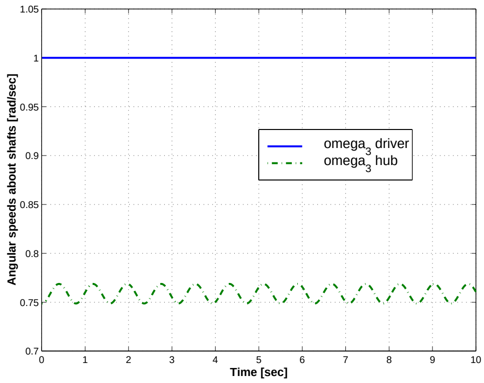

Figure 7: Cone motions (20 deg. semi-aperture): driving shaft angular speed ω_3^d (solid line), slave shaft angular speed ω_3^s (dash-dotted line).

Fig. 6 gives the time history of the shaft rotations, of the universal joint rotations, and of the relative rotation in the revolute joint at A. Fig. 7 gives the time history of the body attached components of angular velocity along the shaft axis and the hub normal. It is seen in this case that the joint does not provide an exact constant speed transmission: the hub rotational speed presents an oscillating behavior, and its mean value is lower than the angular speed of the driving shaft.

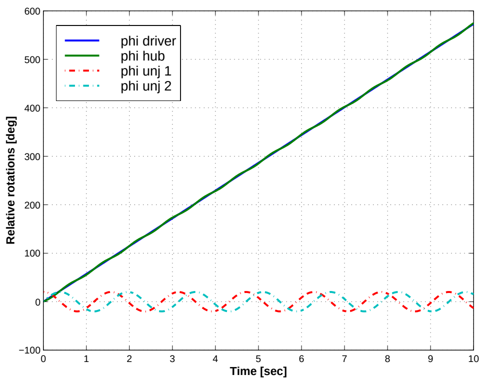

Figure 6: Cone motions (20 deg. semi-aperture): shaft rotations (solid lines), universal joint rotations (dash-dotted lines).

The transmission becomes closer to the constant speed case when the cone semi-aperture is reduced. This is shown if fig. 8, that reports the time history of the angular velocity components for a cone semi-aperture of 5 deg., a value that is more representative of the flapping motions of a rotor. Note that the hub speed oscillations are greatly reduced in this case, and that the velocity mean value is now closer to the driving angular speed.

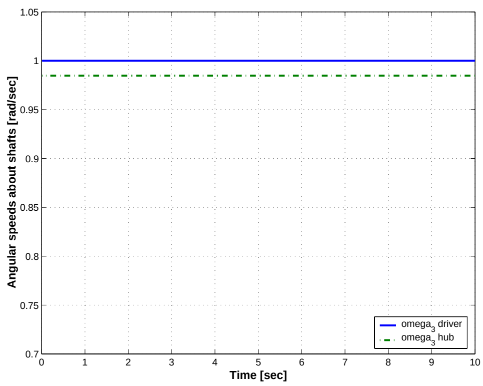

Figure 8: Cone motions (5 deg. semi-aperture): driving shaft angular speed ω_3^d (solid line), slave shaft angular speed ω_3^s (dash-dotted line).

Ideal Constant-Speed Joint Model

The third and final gimbal mount considered in this work is an ideal joint, that guarantees an exact transmission of the driving shaft angular speed to the hub angular speed about its local normal. The other two components of the hub angular velocity are clearly not constrained by the joint, so that the rotor is free to flap.

In a multibody approach, this ideal joint could be enforced as a non-holonomic constraint, equating the two components of angular velocity. In reality, the same effect can also be obtained with a simple modification of the system topology, as depicted in fig. 9. In fact we can take advantage of the fact that the shaft is rigid and that the driving angular speed is constant and known a priori. In this modified model, the shaft now only serves the purpose of driving the scissors that connect to the upper part of the swashplate. The hub is connected to the nacelle through a universal joint that allows its flapping motions. A revolute joint is now introduced between the hub and this universal joint. The relative rotation in the revolute joint can be driven with a linear in time function so as to guarantee the desired value of angular velocity.

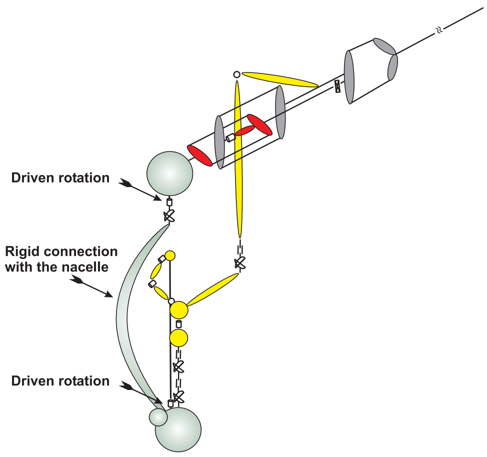

Figure 9: Topological model of the ideal constant speed joint.

Model Validation

Before conducting the aeroelastic simulations, the model was validated against alternative simulation procedures.

Structural Validation

The structural validation was determined first in terms of natural frequencies of the critical system components. The reference code used for the validation is NASTRAN. The NASTRAN model of the blades is extremely similar to the one used for the multibody code, and includes a detailed descriptions of the flex-beam and cuff with multiple load paths.

Nastran	Present
2.74	2.75
4.00	4.00
7.29	7.28
19.08	19.05
25.90	25.93
45.80	45.50

Table 1: Wing eigenfrequencies [Hz].

Table 1 gives the first eigenfrequencies of the wing. Very close agreement is observed for all modes considered. Table 2 gives the first non-rotating eigenfrequencies of the rotor. Even in this case, very close agreement is observed for all modes considered. Table 3 reports the rotating eigenfrequencies in a vacuum for the rotor at a representative airplane mode flight condition. The correlation between the two codes is slightly less satisfactory in this case, in particular for the torsional modes.

	Nastran	Present
Cyclic		
gimbal	0.66	0.66
1 chord	10.33	10.30
1 tors	28.80	28.84
2 tors	42.68	42.63
1 beam	77.59	77.24
Collective		
1 beam	4.25	4.24
1 chord	10.35	10.31
1 tors	33.11	33.16
2 tors	49.54	49.41
2 beam	88.82	89.33

Table 2: Non-rotating eigenfrequencies in airplane mode [Hz].

For the validation effort, a CAMRAD model of the tilt rotor was also prepared. This model uses an equivalent beam for modeling the whole blade system, since multiple load paths are not allowed for this code. In particular, the stiffness and inertial

	Nastran	Present
Cyclic		
gimbal	6.23	6.20
1 chord	11.08	11.04
1 tors	28.99	25.90
2 tors	45.36	44.56
2 beam	79.77	79.26
Collective		
1 beam	7.79	7.71
1 chord	11.10	11.05
1 tors	33.10	30.60
2 tors	51.90	50.91
2 beam	89.95	89.72

Table 3: Rotating eigenfrequencies in airplane mode [Hz].

properties in the area of the flex-beam and cuff are adjusted in order to yield eigenfrequencies similar to those of the detailed model.

Various tests at different rotational speeds were conducted in an effort to try to compare the modeling of the tennis racquet effect in CAMRAD and the present code. In the latter case, the geometrically exact beam theory adopted does not introduce modeling approximations for this potentially important effect.

Fig. 10 shows the pitch distribution along the blade span computed using the two codes. Only the blade is deformable in this case, and infinitely rigid control linkages are used. A somewhat different blade twisting is observed. Fig. 11 shows the results obtained by considering an infinitely stiff blade, but compliant control linkages. This effect is obtained in CAMRAD introducing suitable torsional springs in the pitch hinge, while for the multibody code it is given by the special mechanism described earlier. Even in this case a different behavior is observed, demonstrating a different modeling of the tennis racquet effect in the two codes.

The approximations in the tennis racquet effect modeling in CAMRAD might imply a somewhat different aerodynamic behavior of the rotor, for example in terms of thrust versus power, because of the different pitch settings of the blade sections. This was indeed observed for a number of flight conditions at sea level. The effect is however much

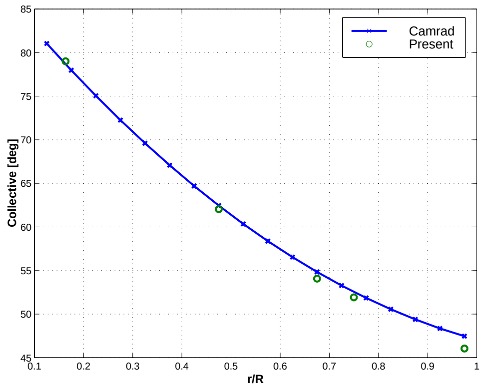

Figure 10: Tennis racquet effect, rigid control linkages and flexible blade: pitch distribution along span.

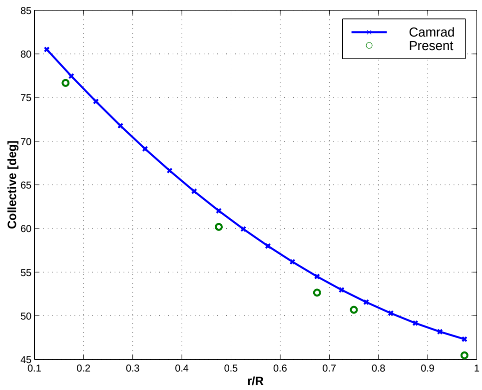

Figure 11: Tennis racquet effect, flexible control linkages and stiff blade: pitch distribution along span.

less pronounced for the flight conditions at 7500 m used for the aeroelastic studies reported here.

Aerodynamic Validation

The aerodynamic validation was conducted by comparison with the CAMRAD code. At first, various trim conditions in airplane mode were computed using CAMRAD for the deformable blades and control linkages model. The nacelle was clamped to the ground during these tests, so that the rotor operates in axial flow. Next, the same pitch control settings computed by CAMRAD were applied to the multibody model. These pitch values were applied to the model by shifting the swashplate along the shaft. Finally, the inertial loads corresponding to the rotation about the shaft axis were applied to the system, together with the corresponding aerodynamic loads. The deflected configuration of the system was consequently computed using the static solution procedure.

Fig. 12 shows the values of thrust and shaft power computed by the two codes at 7500 m of altitude. Very close agreement is observed at all flight conditions considered, except for the last one where the differences in the modeling of the tennis racquet effect induce slight changes in angle of attack of the blade sections. At high values of dynamic pressure, small changes in angle of attack can produce changes in global aerodynamic loads on the rotor which are not totally neglectable.

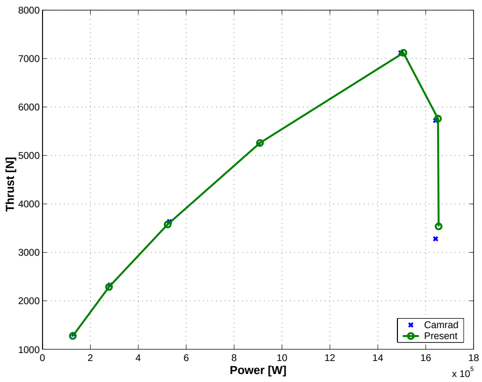

Figure 12: Airplane mode: thrust vs. power at different trim points.

To check the behavior of the two codes for flight conditions which are not in axial flow, an additional test was conducted. In this case the rotor system is fully rigid and flapping at the gimbal joint is prevented. The rotor is then actuated at constant speed at various nacelle tilt values. The global forces and moments on the rotor were then measured and compared between the two codes. Good correlation was observed even in this case for all measured loads at all nacelle tilt angles. For example, fig. 13 gives the H force component (aerodynamic resultant component in the plane of the rotor) versus nacelle tilt.

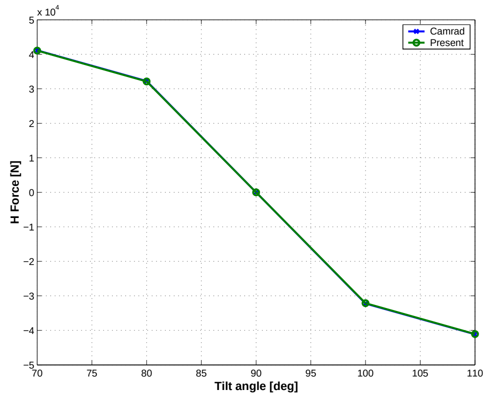

Figure 13: Quasi-static conversion: rotor H force vs. nacelle tilt angle.

Whirl-Flutter Analysis

Analysis Procedure

The flutter analysis was conducted according to the following process.

At first, a static solution procedure applies the pitch control settings for the flight condition under consideration by translating the swashplate as previously discussed. Next, the procedure applies the inertial loads corresponding to the rigid rotation about the shaft and the resulting aerodynamic loads. During this sequence of operations, the rotor is allowed to deform under the applied loads; however, the wing tip is partially clamped to the ground. More precisely, chord and twist rotations are prevented, since these would cause the rotor to leave the axial flow condition.

The equilibrium configuration computed in this way is now used as the initial condition for a transient dynamic analysis. At the beginning of this process, the wing tip clamp is removed. Under the rotor thrust, the wing then deflects and the rotor leaves the axial flow condition. The simulation is then advanced in time for a few complete rotor revolutions.

If the flight condition analyzed is stable, the system will quickly reach a periodic solution, characterized by moderate flapping motions of the rotor. If on the other hand the flight condition is unstable, the system will quickly diverge from the initial condition. In this sense, the initial condition computed by partially clamping the wing provides a simple way of exciting the system to test its stability.

An alternative way of testing the stability of the system is by using Floquet analysis. Using this approach, the periodic equilibrium solution should first be computed. One has then to evaluate the dominant eigenvalues of the the transition matrix that maps initial perturbations of the various degrees of freedom of the system into perturbations after one rotor revolution, perturbations computed starting from the periodic solution. The Arnoldi algorithm provides a way to compute this information even for systems denoted by a considerably large number of degrees of freedom.

When the system is stable, the periodic solution computed as previously discussed provides the initial condition for the Floquet analysis. When the system is unstable, we use the following way of computing the periodic solution. First, the axial flow condition with partially clamped wing tip is computed as previously explained. Next, a transient analysis is started from the results so obtained, removing the wing tip clamp, as before. However, in this case a certain amount of structural damping is introduced in the wing. The damping is progressively increased until one can reach a periodic solution. The introduction of damping is clearly an artificial device that has the only purpose of stabilizing the system. However, its effects on the periodic solution obtained is minimal, since it will only alter the periodic deflections of the wing, which are however very small at trim. Note that no damping is introduced in the rotor, since this might notably change the periodic condition. Once this artificially stabilized periodic condition has been obtained, the structural damping in the wing is removed and the Floquet analysis is conducted.

Results

The whirl-flutter analysis process described so far was applied to the Erica virtual multibody model. A typical solution obtained with the proposed approach is shown in fig. 14. The plot shows the spectral radius of the dominant eigenvalue versus flight speed at 7500 m of altitude. The system is unstable if the spectral radius is larger then one. From the plot, it appears quite clearly that the details of the transmission of motion form the shaft to the hub have a noticeable effect on the stability of

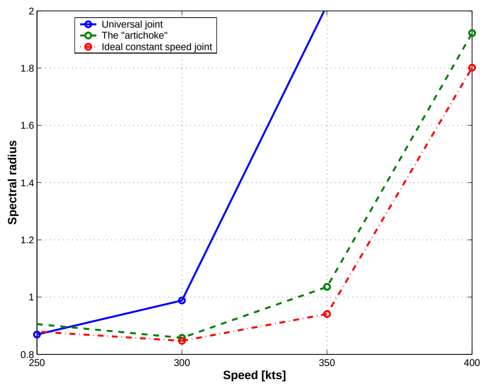

Figure 14: Whirl-Flutter: spectral radius of the transition matrix vs. flight speed for the three joints.

the aircraft. In particular, the universal joint has the lowest flutter speed, while the ideal joint has the highest. The “artichoke” gimbal mount, that approximates quite well an ideal constant speed transmission for small rotor flapping as shown before, behaves better than the universal joint, indeed quite similarly to the ideal one.

To gain a better insight into the mechanism of flutter, the eigenvector associated with the unstable eigenmode can be analyzed. Fig. 15 shows two snap-shots from an animation of the mode. It appears that the instability is caused by a coupling of the wing first bending and torsional modes with lagging and flapping motions of the rotor.

In order to try to corroborate these results, transient analyses were conducted starting from the axial flow, partially clamped conditions, as described above. Fig. 16 shows a few snap-shots obtained from the transient simulation in an unstable regime. The animation shows once again the qualitative nature of the instability, with large bending and torsion of the wing coupled with lag motions of the blades and pronounced flapping of the whole rotor.

Fig. 17 shows the computed time histories of the wing tip displacements for the flight condition at 350 kts. Even using this approach to analyze the system stability, it appears that the three joints behave in markedly different ways. In particular, the universal joint is in a more unstable regime than then the “artichoke” joint, which in turn is more unstable than the ideal joint. Indeed this latter

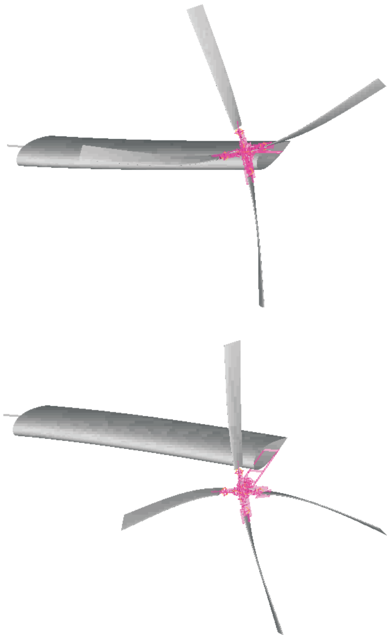

Figure 15: Whirl-Flutter: animation of the dominant eigenmode of the transition matrix (flight condition V=350 kts) for the universal joint.

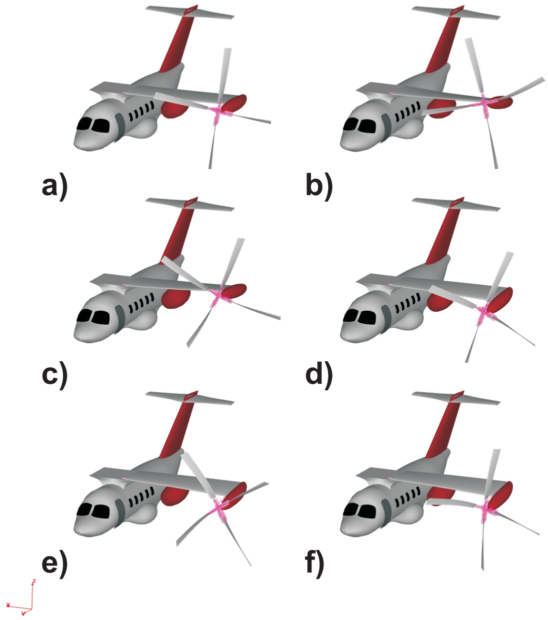

Figure 16: Whirl-Flutter: animation of the transient response in the unstable regime (flight condition V=350 kts) for the universal joint solution.

joint appears to be very near the stability limit, since the wing tip amplitudes grow very slowly.

Comparing with fig. 14, it should be noticed that the Floquet analysis had predicted a stable solution for the ideal joint at 350 kts, prediction which is not here confirmed. There are a few possible explanations for this fact. First, when performing the transient analysis, the excitation was applied to the system not at its periodic solution as in the Floquet case, but starting from the approximate trim in axial flow. Second, this excitation is not guaranteed to be "small", so some system non-linearities might be excited during the process. Third, even the implicit Floquet method needs to perturb the system in order to extract the dominant eigenvalues. If the perturbation is too small, its effects could be masked during the integration of the equations of motion throughout a complete revolution. In fact, the integration is clearly conducted in finite precision arithmetic and requires the solution of non-linear systems of algebraic equations at each time step, which necessarily implies the use of some convergence tolerance. On the other hand, if the perturbation is too large, it can excite the non-linearities present in the system. While due attention was paid to all these issues during the analysis, it is clear that these topics need additional investigation in the future.

The transient simulations were also analyzed in order to try to understand the whirl-flutter instability here found. The global loads applied by the rotor at the wing tip provide some insight on this problem. Fig. 18 shows the time history of the wing tip forces. It appears that the main contributor to the instability is the load promoting beam deflections of the wing. The chord load oscillates about a mean value that is in close agreement with the nominal thrust at this flight condition (fig. 12). Although the gimbal mount has a small amount of flapping stiffness in this rotor, the moments at the wing tips are almost essentially due to the transport of the rotor forces. Even though the three joints studied are clearly different as far as the stability boundaries are concerned, the mechanism of flutter in the three cases does not seem to differ significantly.

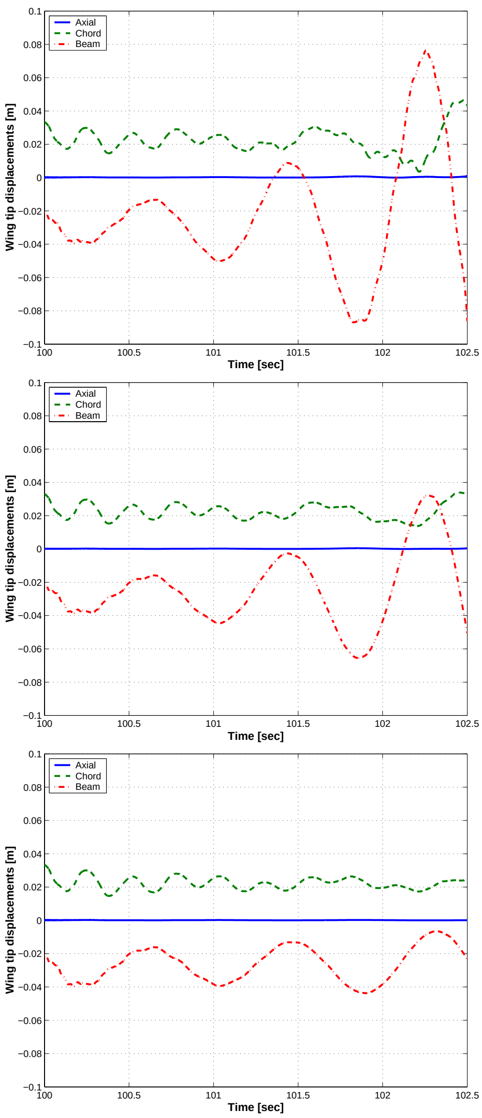

Figure 17: Whirl-Flutter: wing tip deflections vs. time in the unstable regime (flight condition V=350 kts) for the three joints (top to bottom: universal, artichoke, ideal).

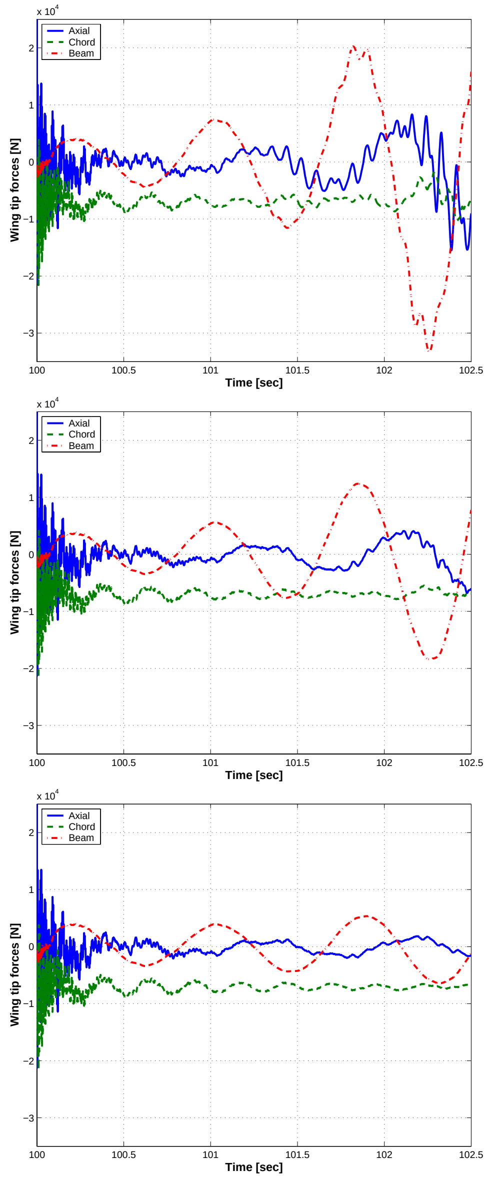

Figure 18: Whirl-Flutter: wing tip total internal reaction forces vs. time in the unstable regime (flight condition V=350 kts) for the three joints (top to bottom: universal, artichoke, ideal).

Conclusions and Future Work

We have studied three alternative design solutions for the gimbal mount. The first uses a simple universal joint, and is representative of the level of detail allowed by other non-multibody based simulation procedures. The second is an approximate constant speed joint, and is representative of a possible actual hardware implementation of this critical component. The third is an ideal joint that guarantees perfect constant speed transmission in all flight conditions, but would clearly be not easy to realize and implement in a real aircraft.

Using these three gimbal mounts, we have conducted a preliminary study of the whirl-flutter boundaries. Stability itself was analyzed in two different ways, by means of transient simulations and by using the implicit Floquet method. Both approaches seem to indicate a progressive increase in the flutter speed associated with a more accurate transmission of the constant speed of the shaft to the hub. The best results were always achieved by the ideal joint, even thought the realizable approximate constant speed joint, here termed the "artichoke", was seen to imply only modest reductions on the flutter boundaries.

We plan to use the tilt rotor model developed herein for a number of further studies. First, a better insight on the stability of the system is necessary. We intend to study the system response to perturbations of variable amplitude, in order to assess the stability "robustness". This study will be conducted perturbing the system starting from the periodic trim conditions, by applying suitable force excitations at the wing tip, similarly to what is done in actual experimental settings. Second, a part from considerations on whirl-flutter stability, a more constant transmission of the angular speed from the shaft to the hub could also have an important impact on the drive train loads and vibratory levels of the aircraft. We intend to investigate these effects by conducting transient simulations for rotors operating at some angle of attack, in order to excite the full rotor dynamics, and by then analyzing the system response in the frequency domain.

The results that were here reported are to be considered preliminary, and further investigations are surely necessary before assessing the true impact of the design details of the constant speed joint on the aeroelastic characteristics of a tilt rotor. Nonetheless, it appears quite clearly even from this preliminary study that modeling assumptions and simplifications in the analysis of these machines in certain flight conditions might severely undermine the accuracy of the computed results. In this sense, the finite element multibody approach seems to offer the potential for enhanced modeling of complex flying machines, by simply providing the tools for a direct numerical simulation of the system components.

Acknowledgments

The first author acknowledges the help of Prof. Olivier A. Bauchau, Georgia Institute of Technology, for the many years of fruitful collaboration on multibody dynamics. The first two authors acknowledge the support of Agusta through contract 01/138/VIL with the Politecnico di Milano.

References

[1] O.A. Bauchau, C.L. Bottasso and Y.G. Nikishkov. Modeling rotorcraft dynamics with finite element multibody procedures. *Math. Comput. Modeling*, **33**:1113–1137, 2001.

[2] O.A. Bauchau, J. Rodriguez and C.L. Bottasso. Modeling of unilateral contact conditions with application to aerospace systems involving backlash, freeplay and friction. *Mech. Res. Comm.*, **28**:571–599, 2001.

[3] O.A. Bauchau and Y.G. Nikishkov. An implicit Floquet analysis for rotorcraft stability evaluation. *J. A. H. S.*, **46**:200–209, 2001.

[4] C.L. Bottasso and O.A. Bauchau. Multibody modeling of engage and disengage operations of helicopter rotors. *J. A. H. S.*, **46**:290–300, 2001.

[5] W. Johnson. CAMRAD/JA: A comprehensive analytical model of rotorcraft aerodynamics and dynamics. Johnson Aeronautics Version. Volume I: Theory manual. 1988.

[6] MSC/NASTRAN Version 70.5 User's Guide.

[7] D.A. Peters and C.J. He. Finite state induced flow models. Part II: Three-dimensional rotor disk. *J. Aircraft*, **32**:323–333, 1995.